

Structure and Residual Stresses in the AMg6 Alloy after Laser Shock Processing

I. A. Bakulin^{a,*}, N. G. Kakovkina^a, S. I. Kuznetsov^a, A. S. Panin^a, and E. Yu. Tarasova^a

^a*Lebedev Physical Institute, Russian Academy of Sciences, Samara Branch, Samara, 443011 Russia*

**e-mail: anton@fian.smr.ru*

Received July 10, 2019; revised November 14, 2019; accepted December 10, 2019

Abstract—The microstructure and distribution of residual stresses in the AMg6 alloy after laser shock treatment in the power density range of 1.3–6 GW/cm² have been studied. Using X-ray structural analysis, it has been found that, after laser exposure, the size of the coherent scattering regions (CSR) decreases to 60 nm, the value of microstrains increases to 0.0018, and the average dislocation density increases from 6.6×10^{13} to 3.7×10^{14} m⁻². Laser shock treatment forms residual compressive stresses to a depth of 1 mm, reaching –128 MPa on the surface of the material.

Keywords: laser shock processing, plastic deformation, dislocations, residual stresses, aluminum alloys

DOI: 10.1134/S2075113321010032

INTRODUCTION

One of the most effective methods for increasing the resistance of materials and products under cyclic loads are surface plastic deformation (peening) by dynamic methods. Mechanical shock, however, has certain disadvantages: the probability of surface cracks, an increase in the surface roughness, a spherical shock front and, as a consequence, a small depth of hardening. As an alternative, back in the 1960s, the idea of the laser shock peening (LSP) was proposed, which has been actively developed over the past 20 years [1–4].

The essence of the technology of laser shock peening consists in the action of a laser pulse with a duration of $\tau = 10$ –50 ns and energy E_{imp} from tenths of a Joule to 100 J on the surface to be treated through a layer transparent to radiation (as a rule, water). As a result of radiation exposure with a power density of $q = 10^9$ – 10^{10} W/cm², a near-surface plasma is formed, which forms a shock wave with a plane front in the material, which creates compression stresses in the surface layer. The transparent layer keeps the plasma from rapid expansion. The depth of peening upon such processing can reach 1.5–2 mm. Laser shock treatment is applied, first of all, to the products made of materials used in the aviation industry: aluminum, titanium, nickel, and magnesium alloys and steels [5–17].

The domestic deformable aluminum-magnesium alloy AMg6 with a magnesium content of 5.8–6.8% has become widespread in various fields of technology. Since AMg6 belongs to alloys that are not hardened by heat treatment, the main way to increase its strength properties are plastic deformation, including bead blasting and ultrasonic treatment.

In this paper, the results of experimental studies of the effect of shock treatment by nanosecond laser pulses on the structure and residual stresses in the AMg6 alloy is presented.

MATERIALS AND METHODS

In the experiments, we used flat samples $15 \times 15 \times 4$ mm in size that was cut from a sheet of polycrystalline industrial alloy AMg6. The composition of the initial samples corresponded to GOST 4784-97; there were no residual stresses on the surface. Before laser treatment, the samples were smoothed using sandpaper and polished using a felt moistened with an aqueous suspension of chromium oxide. Then, electrolytic polishing was carried out for 1–2 min in a solution of perchloric acid HClO₄ in ethyl alcohol (1 : 5). At the final stage, to identify grain boundaries, etching was carried out with Keller's reagent: 10 mL of HF, 15 mL of HCl, 25 mL of HNO₃, 5 mL of H₂O. Then the samples were washed with distilled water and acetone.

The source of pulses was a solid-state YAG: Nd laser LSP 2500 (wavelength is 1.064 μm ; $\tau = 10$ ns; $E_{\text{imp}} = 0.55$ J). The power density q on the sample surface was varied in the range of 1.3–6 GW/cm² by changing the beam diameter using a focusing lens with a focal length of 100 mm.

The samples were processed under 2-mm-thick layer of water with step-by-step displacement with overlapping of the exposure zones by 30–50 % of the laser beam diameter. The plasma cloud was formed in vapors of a specially applied absorbing coating, which was a PVC film 130 μm thick with an adhesive layer and a blue organic pigment. The dark pigment pro-

Table 1. Coefficients of elasticity and compliance in the AMg6 alloy

s_{11} , GPa ⁻¹	s_{12} , GPa ⁻¹	c_{44} , GPa ⁻¹	s_{44} , GPa ⁻¹	$E/(1 + \nu)$, GPa	E/ν , GPa
14.2×10^{-3}	-4.81×10^{-3}	25.9	38.6×10^{-3}	52.4	207

vided a high absorption coefficient for laser radiation with a wavelength of 1.064 μm and zero transmittance. During the experiments, complete penetration of the film and destruction of the polymer from the side of the processed material was not observed.

To determine the microstructure of the materials under study, a Neophot 30 optical microscope, a Carl Zeiss EVO 50 electron microscope and an INCA elemental analysis attachment were used. The microhardness of the materials was measured using a PMT-3 microhardness tester (load weight of 50 g, indentation diagonal of 30–40 μm). X-ray structural analysis was performed on a DRON-3 X-ray diffractometer using $\text{CuK}\alpha$ radiation. Diffraction lines for the analysis of structural changes were recorded point by point with a step of 0.01°. The X-ray beam was formed using Soller slits, horizontal (0.5 mm) and vertical (6 mm) divergence slits, and a receiving slit 0.2 mm wide.

The study of the distribution of residual macrostresses over depth was carried out by layer-by-layer removal of material with a step of 40–100 μm by electrochemical polishing in a solution of perchloric acid HClO_4 in ethanol. The macrostresses in each layer were determined from the shift of the farthest diffraction line of aluminum (511) by the $\sin^2\psi$ method (slope method). In this case, the X-ray beam was formed using horizontal and vertical divergence slits 2 mm in size and a receiving slit 0.5 mm wide. Because of the need to obtain a large amount of experimental data, diffraction peaks were recorded at two slope angles $\psi = 0^\circ$ and 50° at points with a step of 0.02°. A sample of AMg6 annealed at 335°C for 2 h served as a reference. The stresses σ_x and σ_y were determined in the directions along the laser passages and across, respectively. To calculate the stresses, the following expressions from [18] were used:

$$\sigma_\varphi = \frac{E}{1 + \nu} \frac{\varepsilon_{\psi_{50}} - \varepsilon_{\psi_0}}{\sin^2 \psi_{50} - \sin^2 \psi_0},$$

$$\varepsilon = \frac{d - d_0}{d_0},$$

where E is Young's modulus, ν is the Poisson coefficient, ε is the relative change in the interplanar distance, d is the interplanar distance (511) of the processed samples and d_0 is the interplanar distance (511) of the reference.

The values $\frac{E}{1 + \nu}$ and $\frac{E}{\nu}$ for line (511) were calculated in the Reuss approximation [19]:

$$\frac{1 + \nu}{E_{hkl}} = s_{11} - s_{12} - 3\Gamma \left(s_{11} - s_{12} - \frac{1}{2}s_{44} \right),$$

$$-\frac{\nu}{E_{hkl}} = s_{12} + \Gamma \left(s_{11} - s_{12} - \frac{1}{2}s_{44} \right),$$

$$\Gamma = \frac{h^2k^2 + k^2l^2 + l^2h^2}{(h^2 + k^2 + l^2)^2}.$$

In the calculations, the coefficients of elasticity c and compliance s determined for AMg6 in [20] were used (Table 1).

RESULTS AND DISCUSSION

Since under laser shock processing with absorbing coating, the surface temperature of the processed material is lower than the recrystallization temperature, which is confirmed by the absence of melting of the polymer film, changes in the microstructure can be caused only by plastic deformation, the rate of which can reach 10^6 s^{-1} [1, 3].

The grains of the initial AMg6, the sizes of which reach 50 μm , are, as a rule, unequal and elongated parallel to the surface (the texture of deformation as a result of rolling). Optical and scanning electron microscopy did not reveal any noticeable differences between the microstructure of unprocessed and processed samples, the grains of which, after laser exposure, retain their size and shape. Figure 1 shows the microstructure of the near-surface layer after treatment with radiation pulses with a power density of 3.6 GW/cm^2 and overlapping of the affected zones in 40% of the diameter of the laser beam. The grain boundaries are clearly visible, as well as large precipitates of intermetallic compounds and other insoluble compounds. These compounds, according to elemental analysis, have a rather complex composition and include, in addition to Al, most often Mg, Mn, and Fe or Mg, Mn, and Si. Besides, micro- and nanopores appear on the surface of a thin section as a result of chemical etching (Fig. 1b), which are formed at the points of the exit of dislocations and, possibly, dissolved microinclusions.

Figure 2 shows the dependences of the microhardness $\text{HV}_{0.05}$ of the samples treated with radiation with different power densities on the depth. As can be seen from the figure, the maximum microhardness values differ from the microhardness of the initial alloy (750–800 MPa) by 10–15 %, but the spread of values does not allow unambiguous correlation between the microhardness, power density, and the depth of the laser treatment zone.

Thus, visible changes in the structure and values of microhardness do not make it possible to reliably eval-

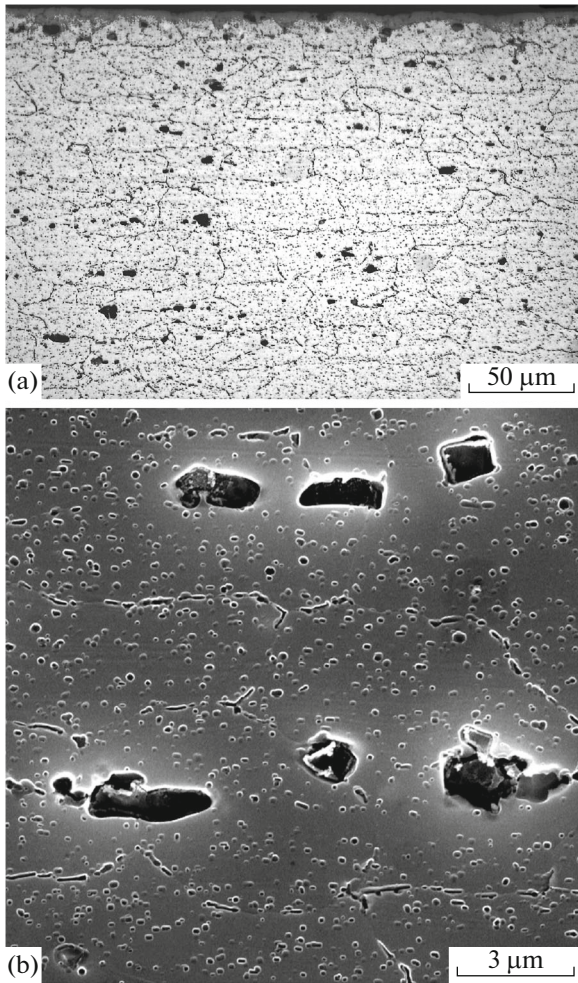


Fig. 1. Microstructure of the AMg6 alloy after processing, $q = 3.6 \text{ GW/cm}^2$: (a) optical microscopy; (b) scanning electronic microscopy.

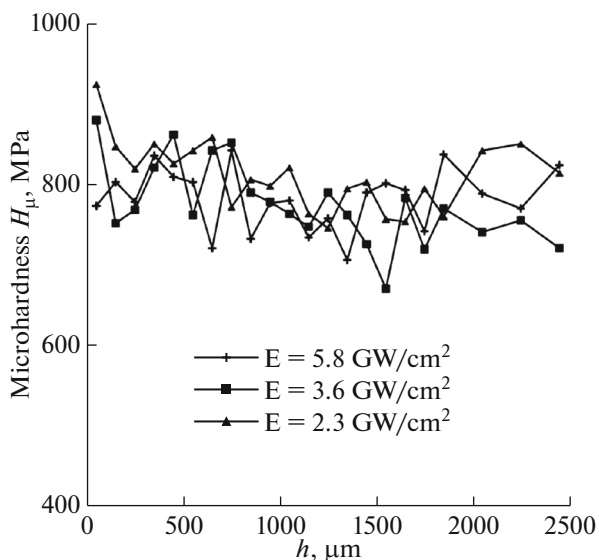


Fig. 2. Microhardness of the AMg6 alloy after treatment at different power density.

uate the results and efficiency of processing and relate them to the parameters of laser shock processing. Information on the phase composition and microstructure of the material can be obtained by methods of X-ray phase and X-ray structural analyses.

Figure 3 shows fragments of X-ray diffraction patterns of the AMg6 sample before and after laser processing with the maximum power density of 5.8 GW/cm^2 . As can be seen from the figure, the ratio of the intensities of diffraction lines of Al after laser irradiation hardly change, which indicates the preservation of the initial textural state of the material and confirms the absence of recrystallization of the surface layer. Both diffraction patterns show lines of intermetallic compounds, which can belong to the systems Al–Mg ($\text{Al}_{12}\text{Mg}_{17}$) and Al–Mn (Al_6Mn , $\text{Al}_{11}\text{Mn}_4$). However, they cannot be identified reliably because of the low intensity of the reflection lines.

The main differences between the diffraction patterns of the treated samples and the diffraction pattern of the initial alloy are the broadening of lines and their shift toward smaller diffraction angles. The line broadening and shift values depend on the radiation power density (Fig. 4), increasing with its increase.

The broadening of diffraction lines is due to a decrease in CSR and an increase in the density of structural defects in the material during its plastic deformation as a result of the pressure of the vapor plasma cloud, which is directly related to the radiation power density [1].

The apparent CSR size D and the value of microstrains ε (averaged over hkl) were determined by analytical formulas in [21], approximating the experimental and instrumental profiles by asymmetric pseudo-Voigt functions. The dislocation densities

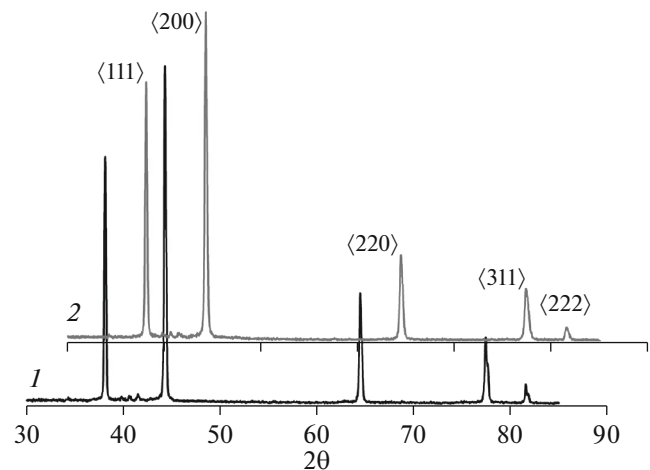


Fig. 3. X-ray diffraction patterns of the AMg6 sample before (1) and after laser processing with power density of 5.8 GW/cm^2 (2).

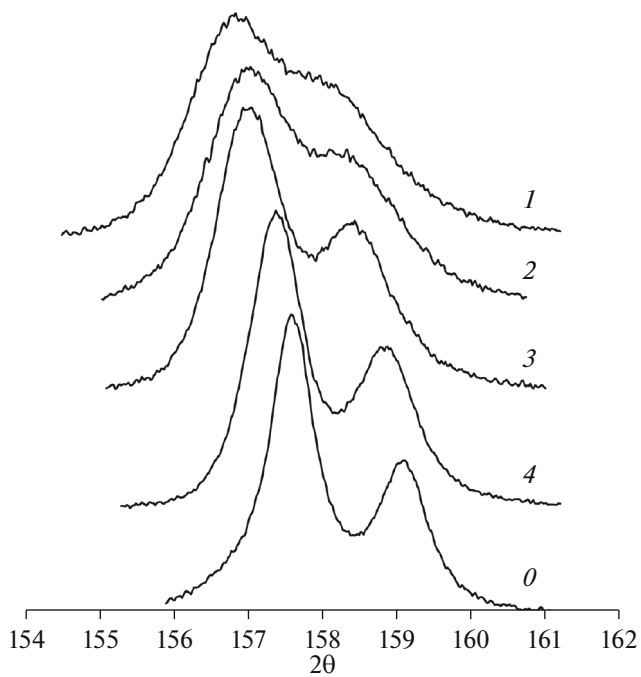


Fig. 4. Diffraction line (511) of the samples processed at different power density of the laser radiation: (0) initial; (1) 5.8; (2) 3.6; (3) 2.3; (4) 1.3 GW/cm².

were calculated according to the formula [22] used in the analysis of plastically deformed fcc metals:

$$\rho = \frac{2\sqrt{3}\epsilon}{bD},$$

where $b = \frac{a}{\sqrt{2}}$ is the modulus of the Burgers vector and a is a parameter of the unit cell. The calculated structural characteristics are given in Table 2 depending on the modes of laser exposure.

According to calculations, the value of microstrains, CSR size, and dislocation density have an explicit dependence on the radiation power density. The values of the structural parameters calculated by X-ray diffraction analysis and their dependence on the energy characteristics of laser shock treatment cor-

Table 2. Dependence of the structural characteristics on the mode of laser impact

q , GW/cm ²	D , nm	$\langle\epsilon\rangle$	ρ , m ⁻²
—	203	0.0011	6.6×10^{13}
5.8	61	0.0018	3.7×10^{14}
3.6	62	0.0016	3.2×10^{14}
2.3	113	0.0013	1.4×10^{14}
1.3	176	0.0011	8.7×10^{13}

relate well with the experimental data of [23], where the microstructure of the 6082 aluminum alloy was studied by transmission electron microscopy after laser shock processing. It is found that the dislocation density after shock treatment increases to $2.9 \times 10^{14} \text{ m}^{-2}$, while the formation of a subgrain structure with dimensions of tens of nanometers is observed.

Note that the profiles of diffraction lines of the annealed sample AMg6 are practically symmetric (with a slight asymmetry due to instrumental distortions). After laser processing, a clear asymmetric broadening of the lines (especially the (200) line) is observed. The asymmetry is the greater, the higher the radiation power density.

The asymmetry of the diffraction peaks is unambiguously associated with defects in the crystal structure. In some cases, in particular, in fcc metals, in which a cellular dislocation structure is possible, the asymmetry of the lines is caused by this structure. In a cellular structure, an asymmetric diffraction line can be represented as a sum of two symmetric lines with different interplanar spacings and different half-widths corresponding to the structure and size of the walls and volume of the cells [24].

To assess the asymmetry of physical diffraction profiles after laser processing, a deconvolution procedure (removal of hardware distortions) was performed; line (200) of annealed AMg6 was used as an apparatus line. Further, the obtained physical line profiles were decomposed into two symmetric subpeaks described by symmetric pseudo-Voigt functions. The positions 2θ , relative intensities I , and half-widths FWHM of subpeaks for the line (200) are given in Table 3.

It can be assumed that, as a result of laser shock treatment, a cellular dislocation structure is formed, which manifests itself in the asymmetry of the (200) line. The first subpeak at $2\theta = 44.30^\circ$ corresponds to the internal volume of cells a larger size and with lower density of dislocations. The second subpeak reflects the size and density of dislocations in the walls of the cells. Note, however, that the formation of a cellular dislocation structure after laser shock processing and the possibility of its analysis by X-ray methods are the subject of thorough separate studies.

Table 3. Characteristics of the subpeaks of the diffraction line (200) depending on the power density of the laser radiation

q , GW/cm ²	First peak			Second peak		
	2θ	I	FWHM	2θ	I	FWHM
—	44.29	1	0.097	—	—	—
5.8	44.31	0.7	0.151	44.23	0.3	0.190
3.6	44.30	0.68	0.104	44.25	0.24	0.145
2.3	44.30	0.73	0.103	44.29	0.29	0.135
1.3	44.30	0.75	0.098	44.34	0.24	0.137

The main task of laser shock treatment from the viewpoint of technological application is to create the required level of residual compressive stresses in the material to the required depth. It is known that in a plane-stressed state, the sign and relative change in the interplanar distance for crystallographic planes parallel to the surface under study depends on the sign and value of the stress, which causes a shift of the corresponding diffraction lines. In this case, the value of the shift is proportional to $\tan \theta$, and its direction is determined by the sign of the stress. The shift of lines in the direction of smaller angles that is recorded in the diffraction patterns, which increases with an increase in the angle of reflection θ , indicates the appearance of compressive stresses at least in the surface layer.

Figure 5 shows distributions of genuine (taking into account the unloading upon removal of the layer) stresses σ_x and σ_y in the treated sample.

Residual stresses, taking into account unloading in the process of the sequential removal of layers for a flat sample, according to [18], were calculated by the formula

$$\sigma(h) = \sigma'(h) - 2 \int_0^h \frac{2b + x - 3h}{(b - x)^2} \sigma(x) dx,$$

where $\sigma(h)$ is the genuine stress in the h layer before the start of bleeding, $\sigma'(h)$ is the stress in the layer at the moment of its exposure (measured stress), b is the sample thickness, and x is the current coordinate. The form of the distribution function of residual stresses in depth $\sigma(x)$ was determined by approximating the experimental points.

As follows from Fig. 5, the area of genuine compressive stresses reaches 1 mm, while the depth of the treated layer exceeds 1.2 mm. A characteristic feature of the used processing scheme is the difference between the values of σ_x and σ_y , where $\sigma_y > \sigma_x$ [25]. In our case, at $q > 2 \text{ GW/cm}^2$, the ratio σ_y/σ_x was in the range of 1.1–1.3.

Figure 6 shows the values of genuine stresses in AMg6 averaged along the x and y axes when processed by radiation with different power densities.

The depth of the region of measured negative stresses in the used range of parameters of the laser shock treatment is in the range of 0.3–1.3 mm, while the depth of genuine negative stresses varies from 0.2 to 1 mm, respectively. There is a clear correlation between the power density and the maximum value of residual stresses: the maximum value of compressive stresses (–128 MPa) corresponds to the maximum value of q . In addition to the power density, the depth of processing is influenced by the diameter of the laser spot on the material surface. The smaller processing depth of sample 1 in comparison with sample 2, despite the higher power density in the first case, is probably due to the smaller diameter of the spot and, as a consequence, less plane shock front in the material.

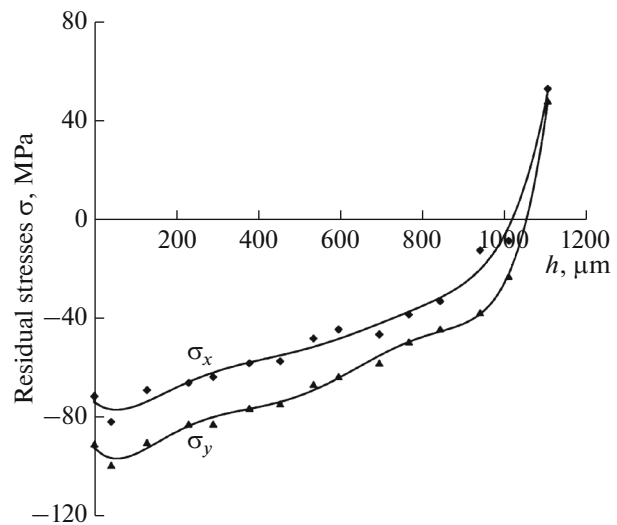


Fig. 5. Distribution of genuine residual stresses σ_x and σ_y in the processed AMg6 sample, $q = 3.6 \text{ GW/cm}^2$.

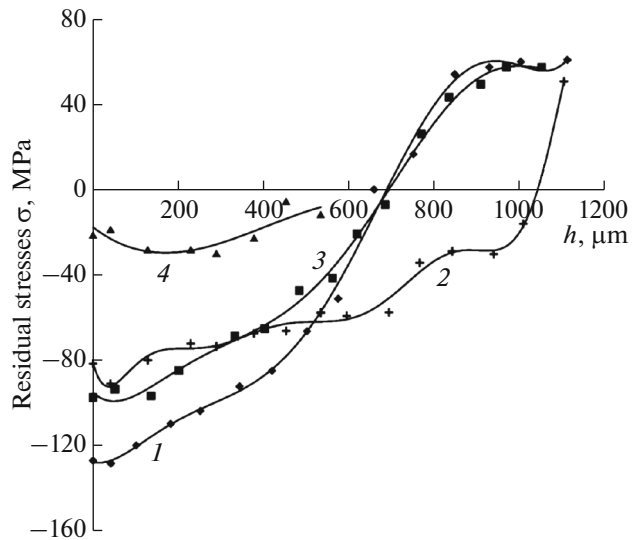


Fig. 6. Distribution of genuine average residual stresses in the AMg6 samples processed at different power density: (1) 5.8; (2) 3.6; (3) 2.3; (4) 1.3 GW/cm^2 .

CONCLUSIONS

The studies have shown that laser shock processing on the surface of the AMg6 aluminum alloy in the power density range of 1.3–6 GW/cm^2 leads to the formation of residual compressive stresses in the material to the depth of at least 1 mm. There is a correlation between the power density and the value of residual stresses: the maximum value of the compressive stresses (–128 MPa) corresponds to the maximum value of q .

Calculations of the dislocation density showed a good correlation with the value of residual stresses on the material surface. In this case, with an increase in

the laser power density, the average dislocation density increases from 6.6×10^{13} to $3.7 \times 10^{14} \text{ m}^{-2}$.

The sizes of the coherent scattering regions decrease to 60 nm with an increase in the radiation power density. The value of microstrains after laser shock treatment increases with increasing power density to 0.0018.

Optical and scanning electron microscopy did not reveal any noticeable changes in the AMg6 microstructure after laser shock treatment. The microhardness of the surface layer of the treated samples is insignificantly (by 10–15 %) higher than the microhardness of the untreated alloy.

REFERENCES

- Gujba, A.R. and Medraj, M., Laser peening process and its impact on materials properties in comparison with shot peening and ultrasonic impact peening, *Materials*, 2014, vol. 7, pp. 7925–7974.
- Chupakhin, S., Klusemann, B., Huber, N., and Kashae, N., Application of design of experiments for laser shock peening process optimization, *Int. J. Adv. Manuf. Technol.*, 2019, vol. 102, nos. 5–8, pp. 1567–1581.
- Sundar, R., Ganesh, P., Gupta, R.K., Ragvendra, G., Pant, B.K., Kain, V., Ranganathan, K., Kaul, R., and Bindra, K.S., Laser shock peening and its applications: a review, *Lasers Manuf. Mater. Process.*, 2019, vol. 6, pp. 424–463.
<https://doi.org/10.1007/s40516-019-00098-8>
- Karthik, D. and Swaroop, S., Laser peening without coating—an advanced surface treatment: A review, *Mater. Manuf. Process.*, 2016, vol. 32, pp. 1565–1572.
- Kashae, N., Ventzke, V., Horstmann, M., Chupakhin, S., Riekehr, S., Falck, R., Maawad, E., Staron, P., Schell, N., and Huber, N., Effects of laser shock peening on the microstructure and fatigue crack propagation behaviour of thin AA2024 specimens, *Int. J. Fatigue*, 2017, vol. 98, pp. 223–233.
- Bergant, Z., Trdan, U., and Grum, J., Effects of laser shock processing on high cycle fatigue crack growth rate and fracture toughness of aluminium alloy 6082 T651, *Int. J. Fatigue*, 2016, vol. 87, pp. 444–455.
- Irizalp, S.G. and Saklakoglu, N., High strength and high ductility behavior of 6061–T6 alloy after laser shock processing, *Opt. Lasers Eng.*, 2016, vol. 77, pp. 183–190.
- Guo, W., Sun, R., Song, B., Zhu, Y., Li, F., Che, Z., Bo, L., Guo, C., Liu, L., and Peng, P., Laser shock peening of laser additive manufactured Ti6Al4V titanium alloy, *Surf. Coat. Technol.*, 2018, vol. 349, pp. 503–510.
- Hongchao, Q., Experimental investigation of laser peening on Ti17 titanium alloy for rotor blade applications, *Appl. Surf. Sci.*, 2015, vol. 351, pp. 524–530.
- Jia, W., Hong, Q., Zhao, H., Li, L., and Han, D., Effect of laser shock peening on the mechanical properties of a near- α titanium alloy, *Mater. Sci. Eng., A*, 2014, vol. 606, pp. 354–359.
- Telang, A., Gill, A.S., Teysseyre, S., Mannava, S.R., Qian, D., and Vasudevan, V.K., Effects of laser shock peening on SCC behavior of Alloy 600 in tetrathionate solution, *Corros. Sci.*, 2015, vol. 90, pp. 434–444.
- Prabhakaran, S. and Kalainathan, S., Warm laser shock peening without coating induced phase transformations and pinning effect on fatigue life of low-alloy steel, *Mater. Des.*, 2016, vol. 107, pp. 98–107.
- Prabhakaran, S., Kulkarni, A., Vasanth, G., Kalainathan, S., Shukla, P., and Vasudevan, V.K., Laser shock peening without coating induced residual stress distribution, wettability characteristics and enhanced pitting corrosion resistance of austenitic stainless steel, *Appl. Surf. Sci.*, 2018, vol. 428, pp. 17–30.
- Gill, A.S., Telang, A., and Vasudevan, V.K., Characteristics of surface layers formed on inconel 718 by laser shock peening with and without a protective coating, *J. Mater. Process. Technol.*, 2015, vol. 225, pp. 463–472.
- Wang, C., Shen, X.J., An, Z.B., Zhou, L.C., and Chai, Y., Effects of laser shock processing on microstructure and mechanical properties of K403 nickel-alloy, *Mater. Des.*, 2016, vol. 89, pp. 582–588.
- Kattoura, M., Mannava, S.R., Qian, D., and Vasudevan, V.K., Effect of laser shock peening on elevated temperature residual stress, microstructure and fatigue behavior of ATI 718Plus alloy, *Int. J. Fatigue*, 2017, vol. 104, pp. 366–378.
- Ge, M.-Z. and Xiang, J.-Y., Effect of laser shock peening on microstructure and fatigue crack growth rate of AZ31B magnesium alloy, *J. Alloys Compd.*, 2016, vol. 680, pp. 544–552.
- Vasil'ev, D.M., X-ray analysis of stress distribution along the section of a product, *Zavod. Lab.*, 1966, vol. 32, no. 6, pp. 708–711.
- Shermergor, T.D., *Teoriya uprugosti mikroneodnorodnykh sred* (Elasticity Theory of Microheterogeneous Materials), Moscow: Nauka, 1977.
- Volkov, A.D., Kokshaiskii, A.I., Korobov, A.I., and Prokhorov, V.M., Second- and third-order elastic coefficients in polycrystalline aluminum alloy AMg6, *Acoust. Phys.*, 2015, vol. 61, no. 6, pp. 651–656.
- Pantoja-Cortés, J., Sánchez-Bajo, F., and Ortiz, A.L., A line-broadening analysis model for the microstructural characterization of nanocrystalline materials from asymmetric x-ray diffraction peaks, *J. Phys.: Condens. Matter*, 2012, vol. 24, pp. 215301–215307.
- Ortiz, A.L., Tian, J.W., Villegas, J.C., Shaw, L.L., and Liaw, P.K., Interrogation of the microstructure and residual stress of nickel-base alloy subjected to surface severe plastic deformation, *Acta Mater.*, 2008, vol. 56, pp. 413–426.
- Trdan, U., Skarba, M., and Grum, J., Laser shock peening effect on the dislocation transitions and grain refinement of Al–Mg–Si alloy, *Mater. Charact.*, 2014, vol. 97, pp. 57–68.
- Mughrabi, H., Dislocation wall and cell structures and long-range internal stresses in deformed metal crystals, *Acta Metall.*, 1983, vol. 31, no. 9, pp. 1367–1379.
- Correa, C., Peral, D., Porro, J.A., Díaz, M., Ruiz de Lara, L., García-Beltrán, A., and Ocaña, J.L., Random-type scanning patterns in laser shock peening without absorbing coating in 2024–T351 Al alloy: a solution to reduce residual stress anisotropy, *Opt. Laser Technol.*, 2015, vol. 73, pp. 179–187.

Translated by Sh. Galyaltdinov